

Electronic Supplementary Information

For

**Antiproliferative Activity of Cationic and Neutral
thiosemicarbazone Copper(II) Complexes**

M. Mohamed Subarkhan,^a Rupesh N. Prabhu,^b R. Raj Kumar^a and R. Ramesh,^{a,*}

^a School of Chemistry, Bharathidasan University, Tiruchirappalli 620 024, Tamil Nadu, India.

^b School of Chemistry, University of Hyderabad, Hyderabad 500 046, Telangana, India.

*To whom correspondence should be addressed, e-mail: ramesh_bdu@yahoo.com, Fax: +91 431 2407045

Table S1. Selected bond lengths [Å] and bond angles [deg]

| | Complex 1 | Complex 3 ·DMF·H ₂ O |
|--------------|------------------|--|
| Cu–O(1) | 1.881(3) | 1.909(3) |
| Cu–N(1) | 1.955(3) | 1.965(4) |
| Cu–S | 2.2370(13) | 2.2121(15) |
| Cu–O(2) | 1.993(3) | |
| Cu–Cl | | 2.2649(15) |
| C(8)–N(1) | 1.292(5) | 1.308(6) |
| N(1)–N(2) | 1.372(4) | 1.374(5) |
| C(9)–N(2) | 1.313(5) | 1.308(6) |
| C(9)–S | 1.745(4) | 1.731(5) |
| O(1)–Cu–N(1) | 94.02(12) | 91.80(15) |
| N(1)–Cu–S | 86.70(10) | 85.68(12) |
| O(2)–Cu–S | 91.80(9) | |
| O(1)–Cu–O(2) | 87.10(11) | |
| Cl–Cu–S | | 92.16(6) |
| O(1)–Cu–Cl | | 91.57(11) |
| O(1)–Cu–S | 176.86(8) | 170.61(11) |
| N(1)–Cu–O(2) | 172.81(12) | |
| N(1)–Cu–Cl | | 171.62(12) |

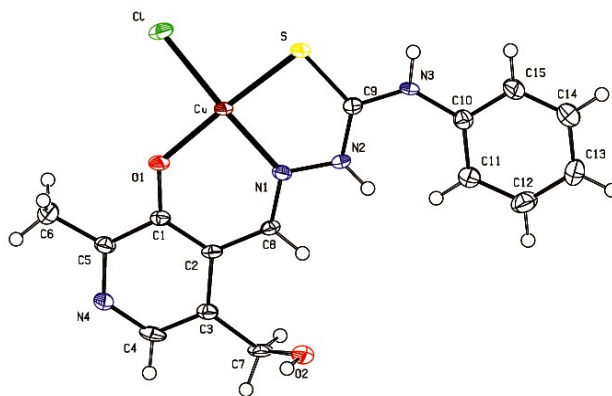


Figure S1. ORTEP view of complex **3** showing thermal ellipsoids at the 30% probability level. Solvent molecules omitted for clarity.

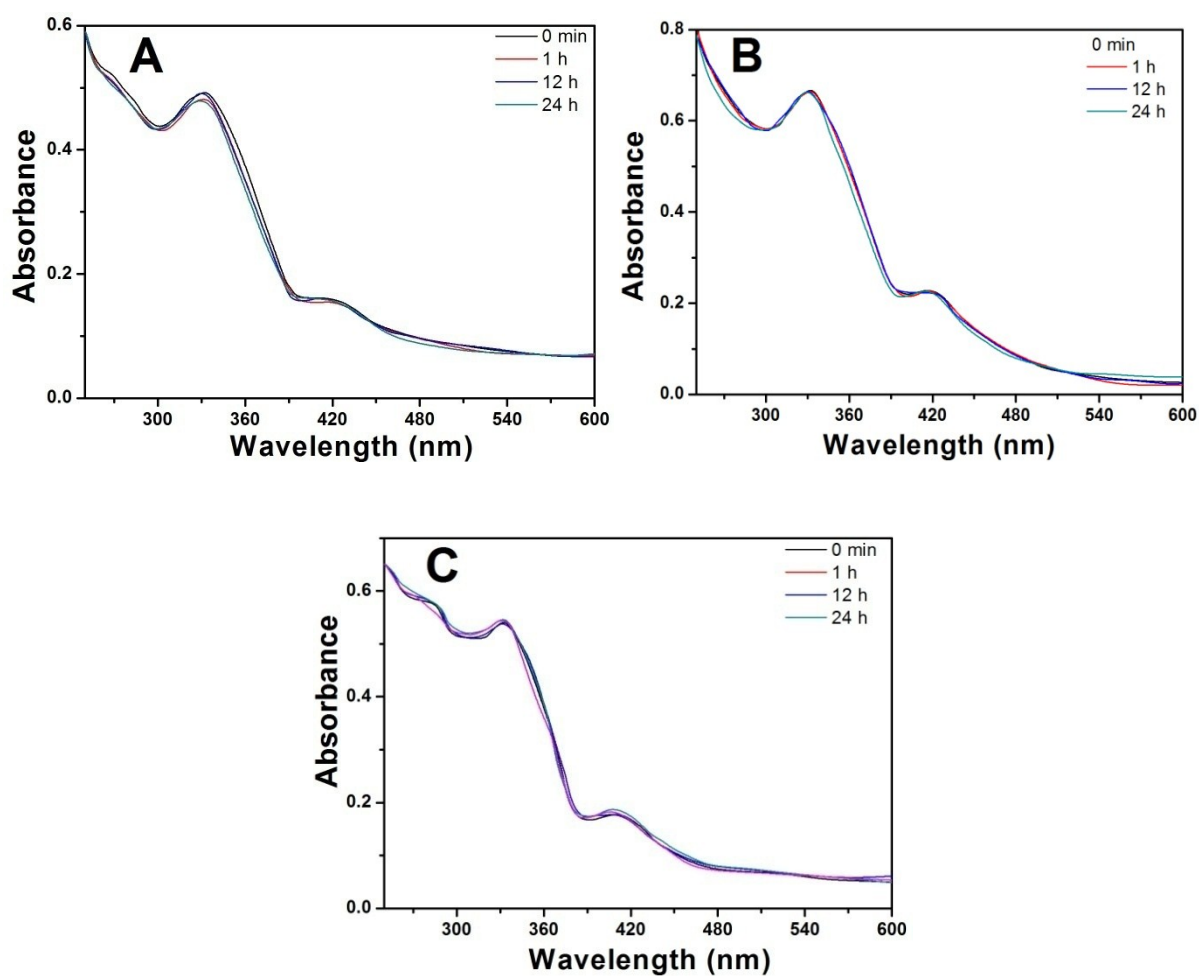
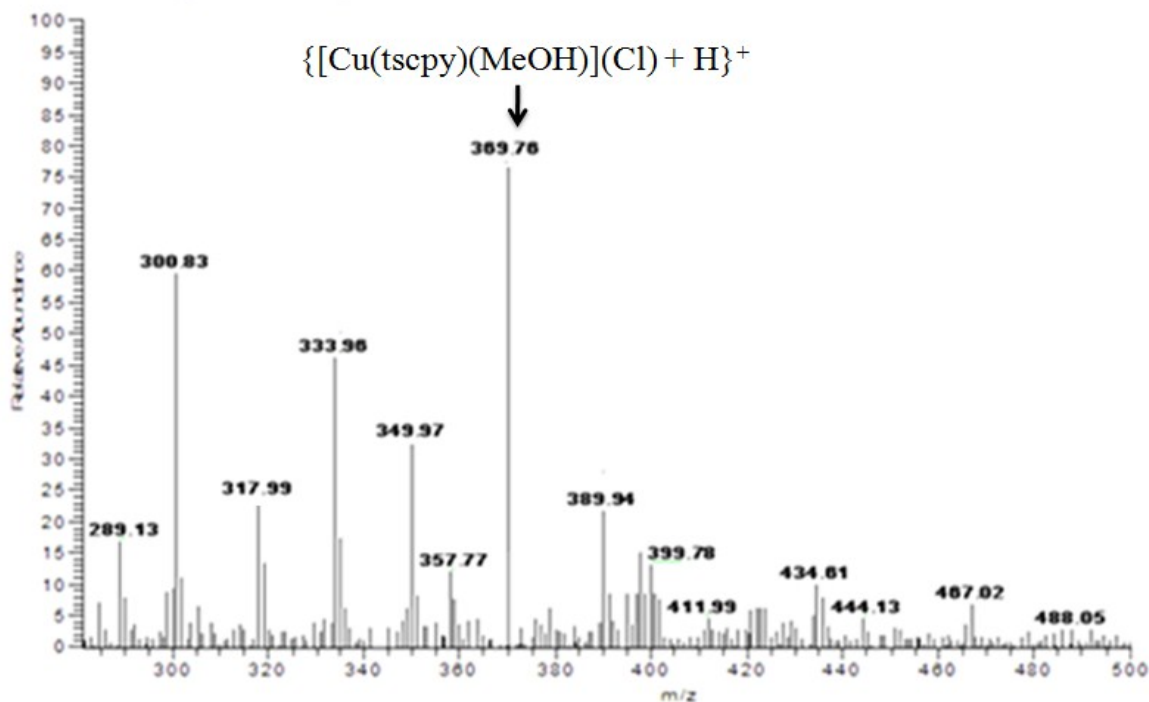
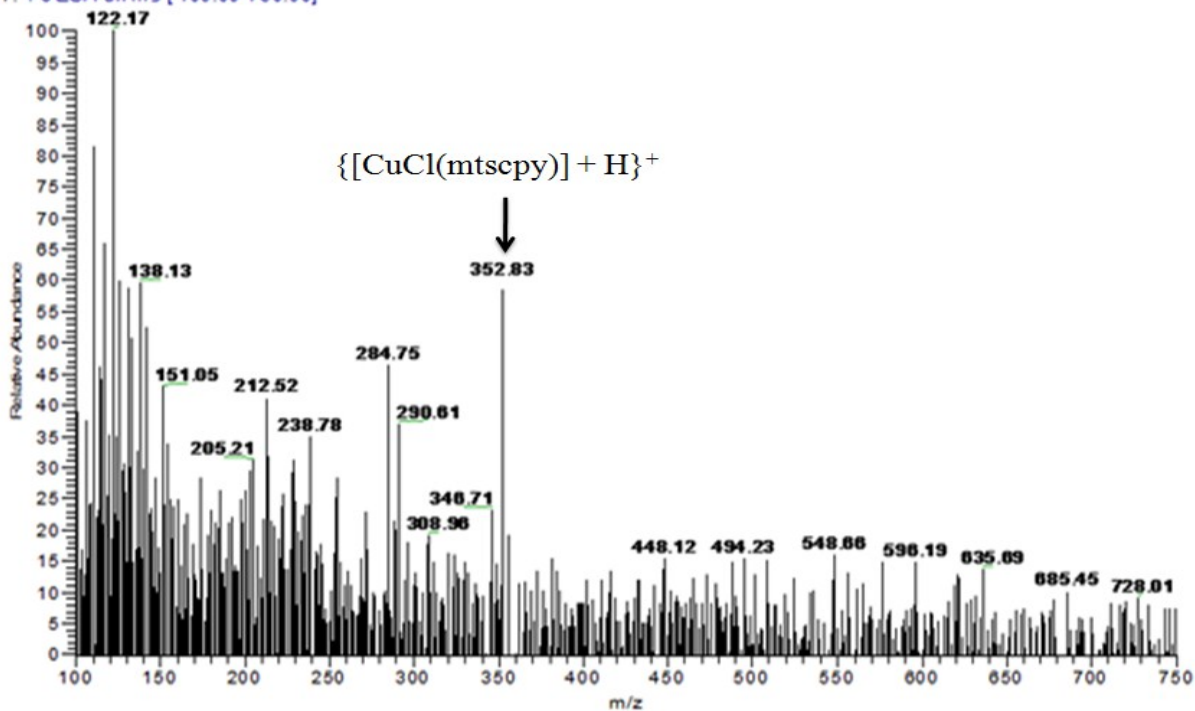


Figure S2. UV-Vis. absorption spectrum of complexes **1(A)**, **2(B)** and **3(C)** in aqueous PBS buffer (phosphate buffered saline solution), at pH 7.4, to a final concentration of 1×10^{-3} M recorded after different time intervals.

30-56 RT: 0.36-0.67 AV: 27 SB: 16 0.09-0.16 , 0.97-1.07 NL: 1.86E7
T: + c ESI Full ms [100.00-500.00]



#30-56 RT: 0.36-0.67 AV: 27 SB: 16 0.09-0.16 , 0.97-1.06 NL: 3.01E6
T: + c ESI Full ms [100.00-750.00]



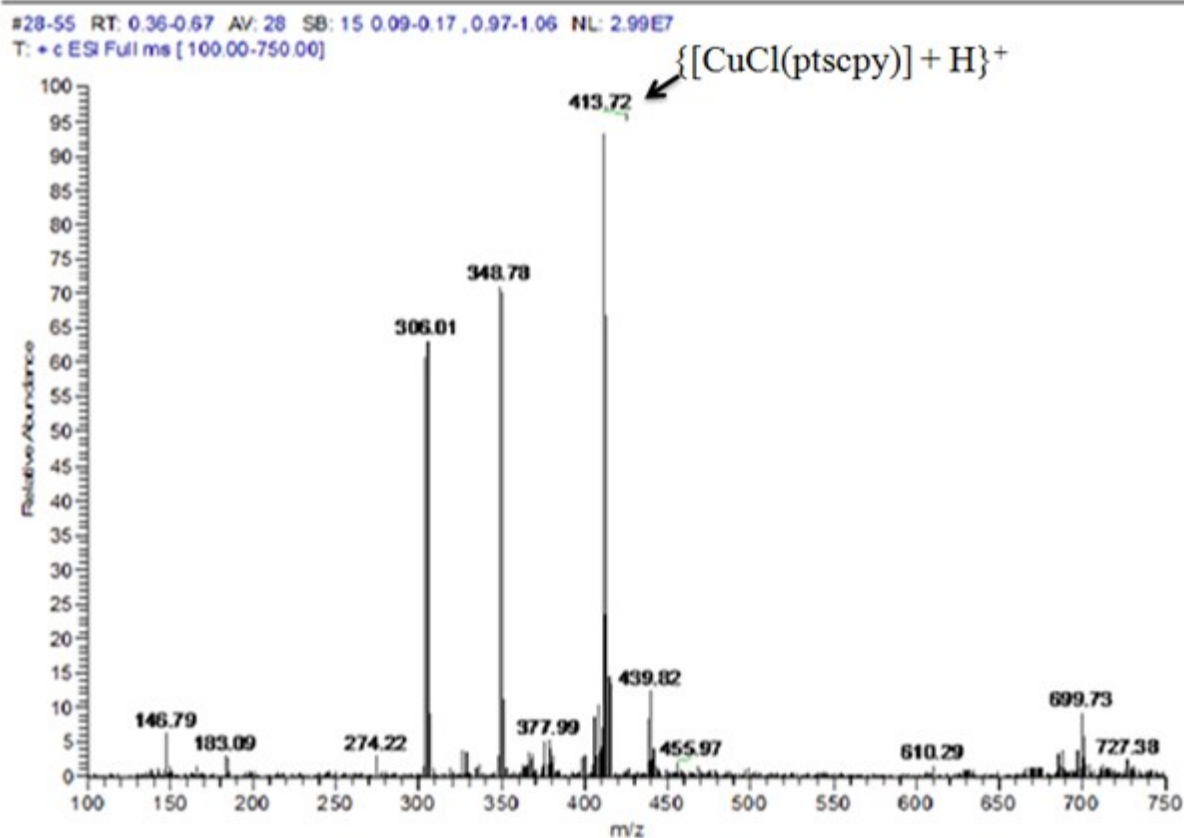


Figure S3. ESI-MS spectra of $\{[\text{Cu}(\text{tscpy})(\text{MeOH})(\text{Cl})+\text{H}]\text{(1)}$, $[\text{CuCl}(\text{mtscpy})+\text{H}]\text{(2)}$ and $[\text{CuCl}(\text{ptscpy})+\text{H}]\text{(3)}\}$ in acetonitrile.

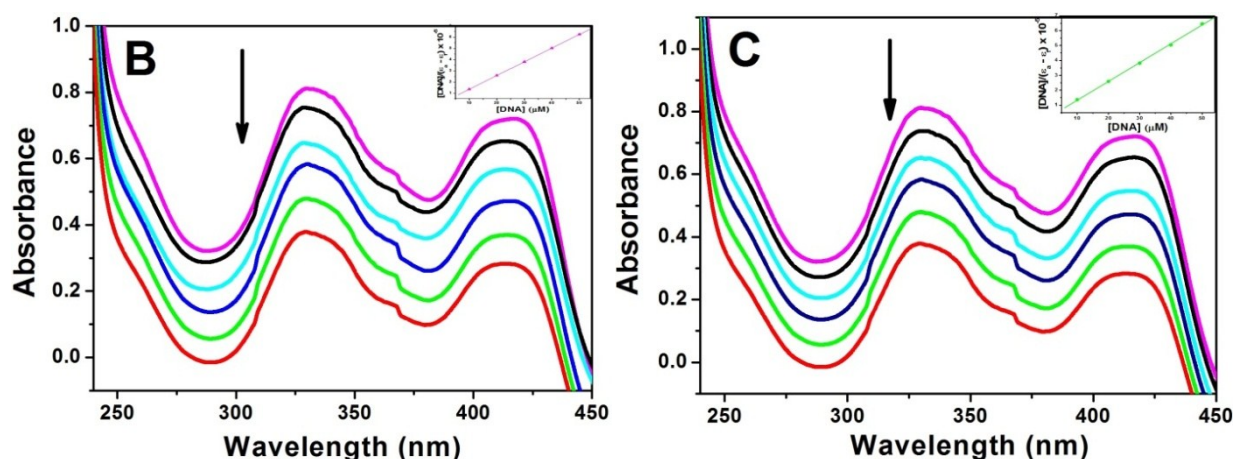


Figure S4. Electronic spectra of complexes **2** (B) and **3** (C), in Tris-HCl buffer upon addition of CT-DNA. $[\text{Complex}] = 25 \mu\text{M}$, $[\text{DNA}] = 0\text{--}50 \mu\text{M}$. Arrow shows the absorption intensities decrease upon increasing DNA concentration. (Inset) Plots of $[\text{DNA}]/(\epsilon_a - \epsilon_f)$ versus $[\text{DNA}]$ for complexes **2** and **3** with CT-DNA.

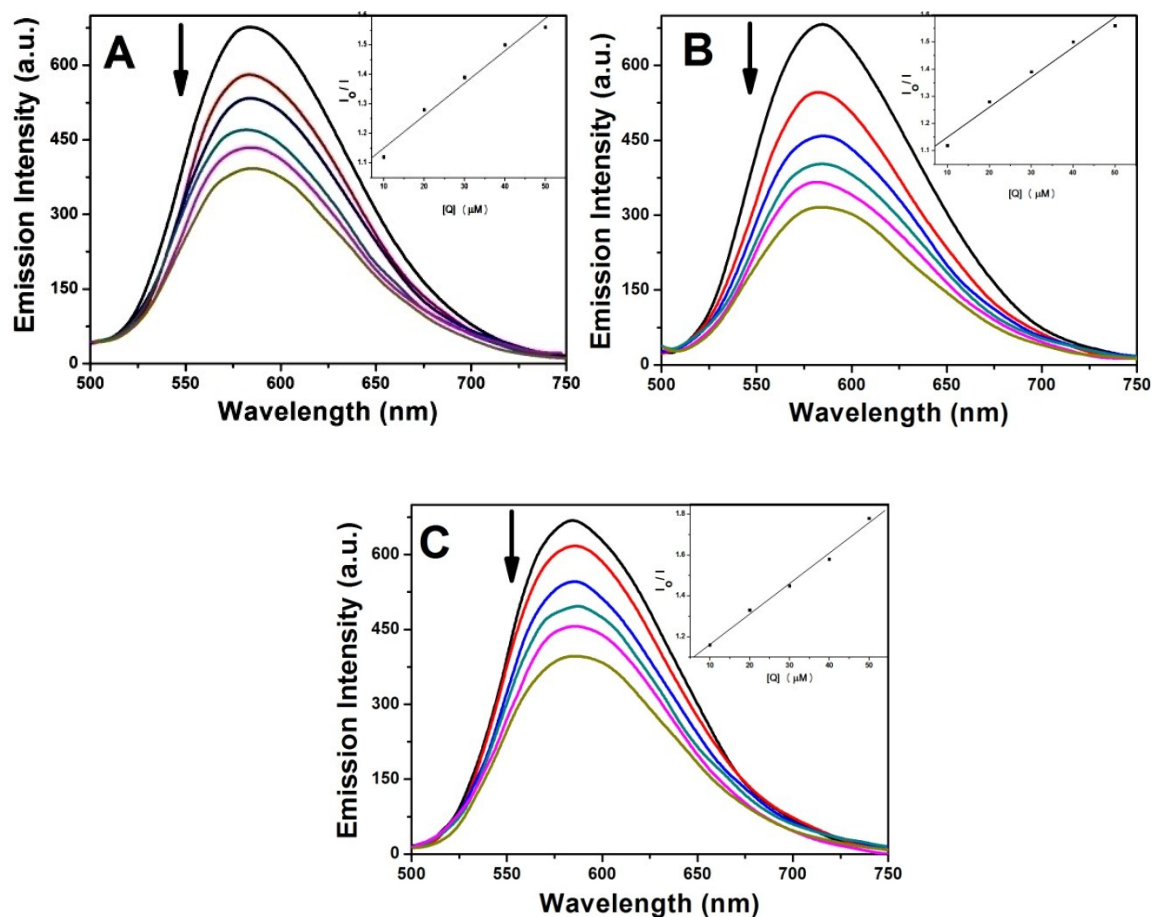


Figure S5. Emission titrations of complexes **1** (A), **2** (B) and **3** (C) with EB bound to DNA, $\lambda_{\text{ex}} = 546 \text{ nm}$, $\lambda_{\text{em}} = 599 \text{ nm}$, $[\text{DNA}] = 12 \mu\text{M}$, $[\text{Complex}] = 0\text{-}25 \mu\text{M}$, $[\text{EB}] = 12 \mu\text{M}$. Arrow shows that the emission intensity changes upon increasing complex concentration. Inset: Stern–Volmer plots of the EB–DNA fluorescence titration for complexes **1**, **2** and **3**.

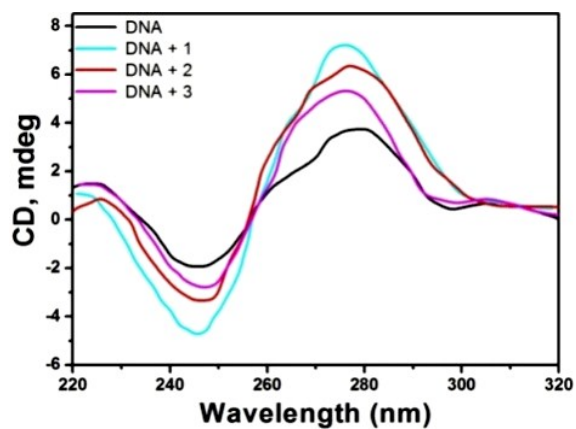


Figure S6. The circular dichroism spectra of free CT–DNA ($10 \mu\text{M}$) and after the addition of complexes **1–3** ($10 \mu\text{M}$).

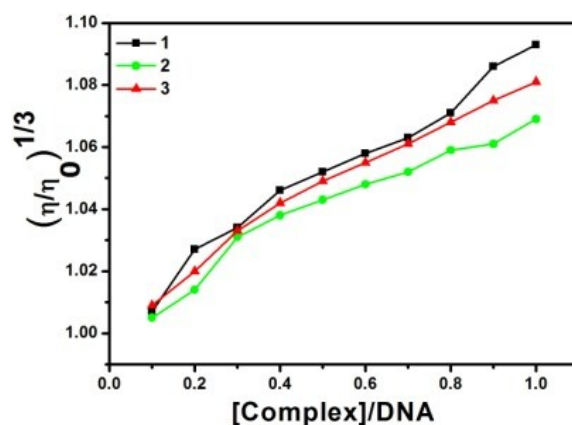


Figure S7. Relative viscosities of CT-DNA in the presence of the complexes 1–3

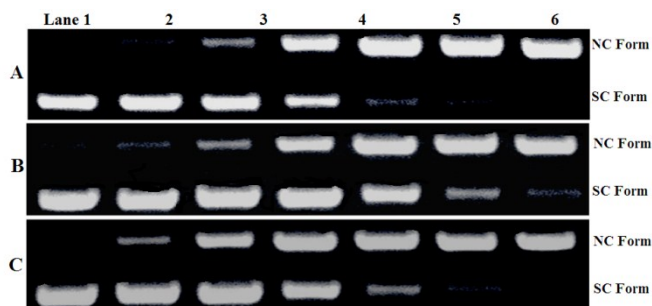


Figure S8. Agarose gel electrophoresis pattern for the cleavage of pUC19 DNA by complexes 1-3 at 37°C after incubation for 1 h. (A), (B) and (c) at different concentrations of 1; lane 1: DNA control; lane 2: 5 μM complex (1), (2) and (3) + DNA; lane 3: 10 μM complex (1), (2) and (3) + DNA; lane 4: 15 μM complex (1), (2) and (3) + DNA; lane 5: 20 μM complex (1), (2) and (3) + DNA; lane 6: 25 μM complex (1), (2) and (3) + DNA; lane 7: 30 μM complex (1), (2) and (3) + DNA respectively.

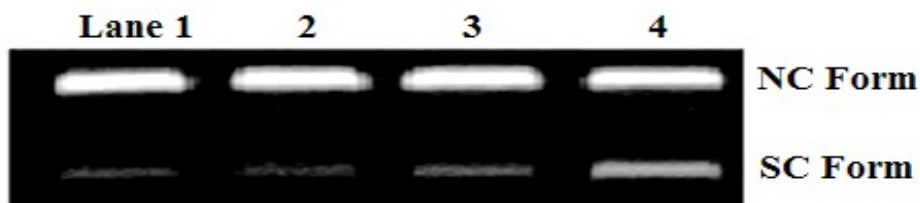


Figure S9. Agarose gel electrophoresis pattern for the supercoiled (SC) pUC19 DNA linearized by complex 1 (25 μM) without reductant after incubation: Lane 1, (100 μM) NaN₃ + 1; Lane 2, (4 units) superoxide dismutase + 1; Lane 3, (10%) DMSO + 1, Lane 4, ethanol + 1.

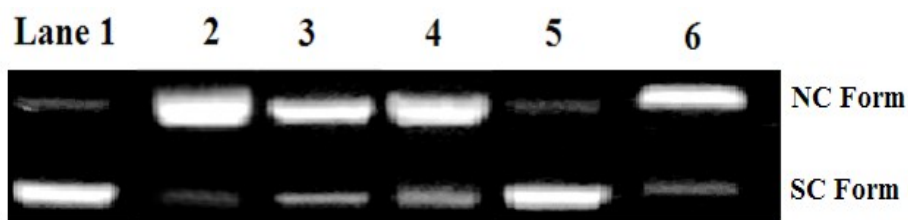


Figure S10. Agarose gel electrophoresis pattern for the ligation of supercoiled (SC) pUC19 DNA linearized by complexes **1-3**: Lane 1, DNA control; Lane 2-4, pUC19 supercoiled DNA cleaved by complex **1-3**; Lane 5, ligation of linearized pUC19 supercoiled DNA by T4 DNA ligase, Lane 6, pUC19 supercoiled DNA cleaved by with adding H₂O₂ T4 DNA ligase.

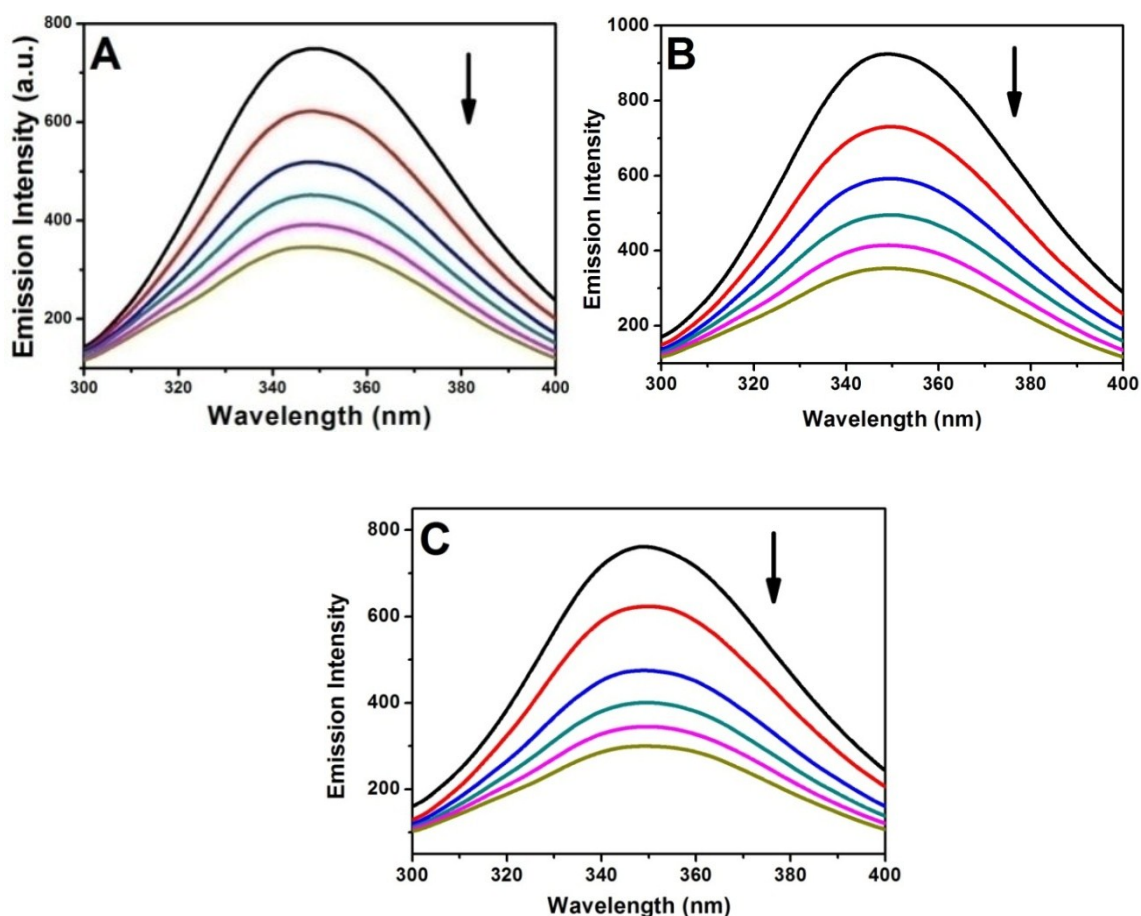


Figure S11. Emission spectrum of BSA (1 μM ; $\lambda_{\text{ex}} = 280 \text{ nm}$; $\lambda_{\text{em}} = 349 \text{ nm}$) in the presence of increasing amounts of complexes **1** (A), **2** (B) and **3** (C) (0–25 μM). Arrow shows that the emission intensity changes upon increasing complex concentration.

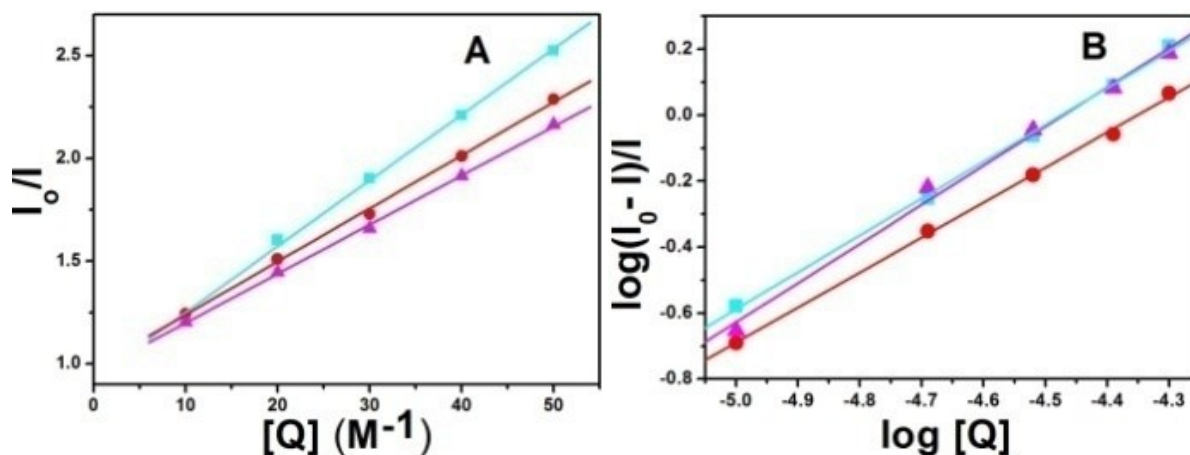


Figure S12. Stern–Volmer (A) and Scatchard (B) plots of the BSA fluorescence titration for complexes 1–3.

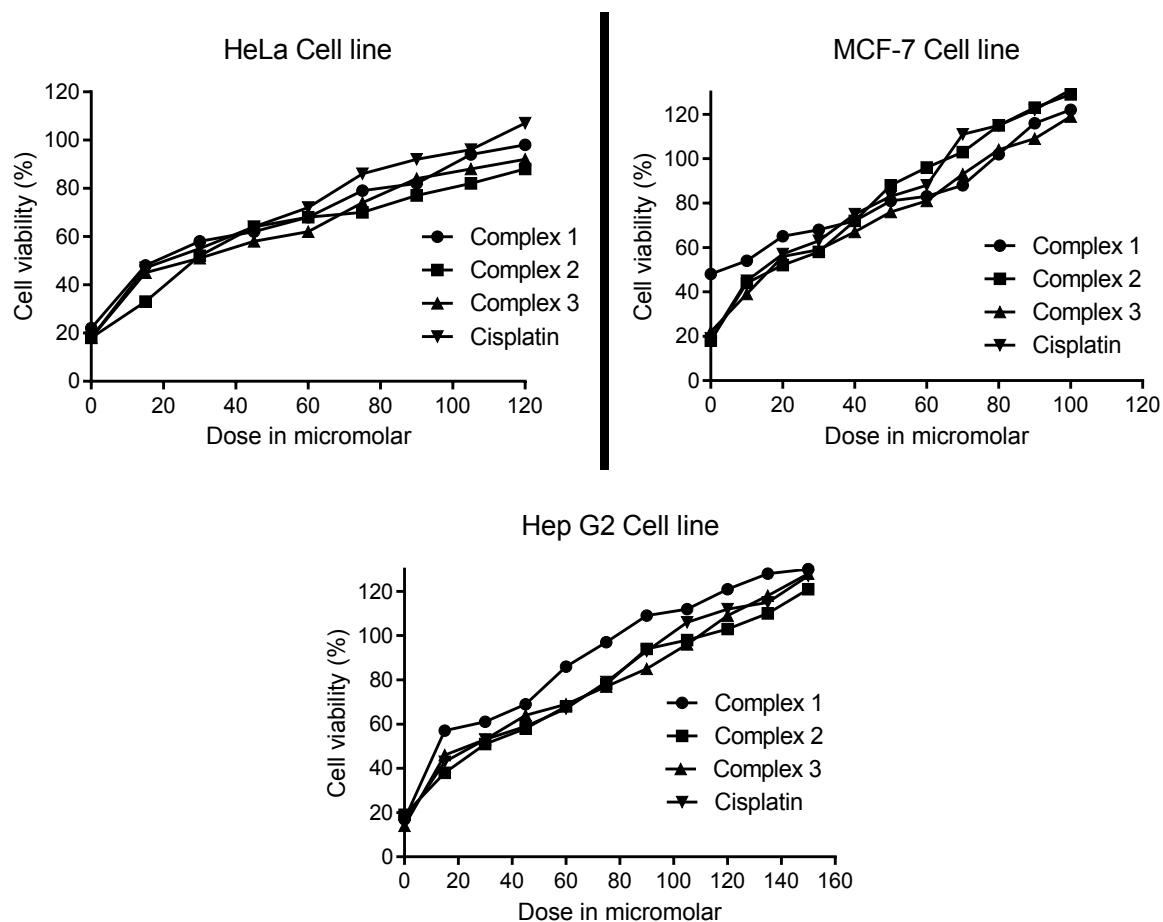


Figure S13. Cell viability plots showing the cytotoxic effect of the complexes 1-3, in HeLa, MCF-7 and Hep G2 cancer cell lines.

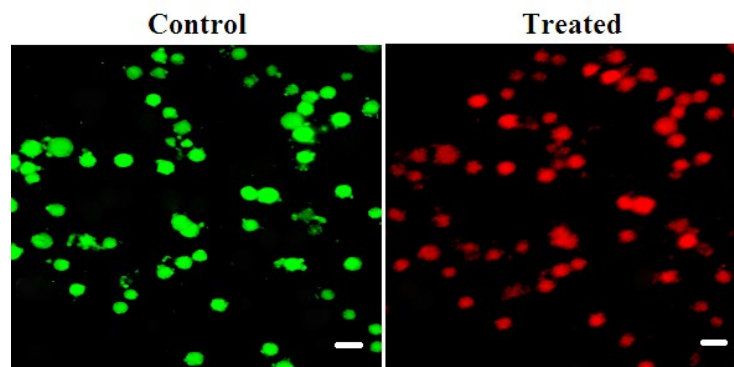


Figure S14. Fluorescence microscope images of Annexin V-FITC staining with MCF-7 cells treated with complex **1** (IC_{50} concentration) for 24 h. The scale bar 20 μm

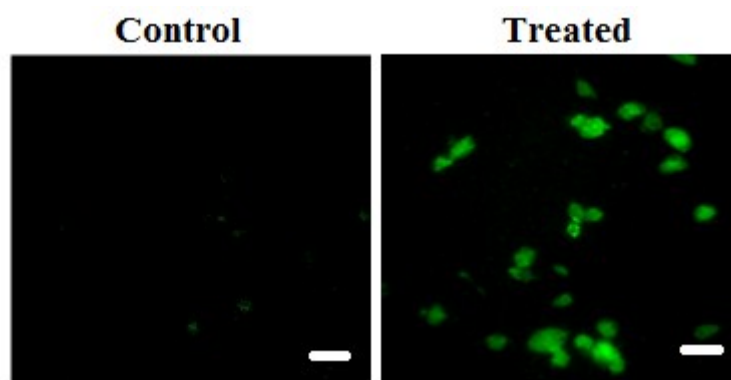


Figure S15. Reactive oxygen species level in MCF-7 cells against complex **1** (IC_{50} concentration) for 24 h. The scale bar 20 μm

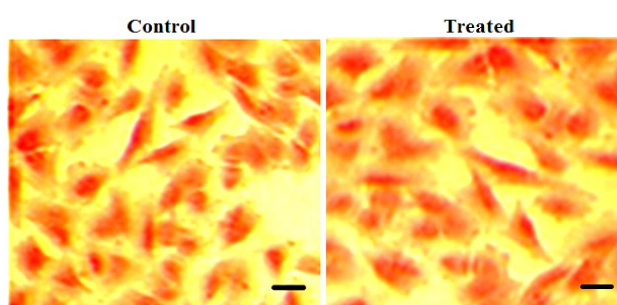


Figure S16. TUNEL assay of NIH 3T3 cells were treated with complex **1** for 24 h. The scale bar 40 μm .